Composite Structures 160 (2017) 89–99

Contents lists available at ScienceDirect

Composite Structures

journal homepage: www.elsevier.com/locate/compstruct

A comparative study of the mechanical properties and failure behavior of carbon fiber/epoxy and carbon fiber/polyamide 6 unidirectional composites

Yan Ma [a], Masahito Ueda [b], Tomohiro Yokozeki [c], Toshi Sugahara [d], Yuqiu Yang [e,*], Hiroyuki Hamada [a]

[a] Advanced Fibro-Science, Kyoto Institute of Technology, Kyoto 606-8585, Japan
[b] Department of Mechanical Engineering, College of Science and Technology, Nihon University, Tokyo 101-8308, Japan
[c] Department of Aeronautics and Astronautics, The University of Tokyo, Tokyo 113-8656, Japan
[d] Maruhachi Corporation, Fukui 910-0276, Japan
[e] Key Laboratory of Textile Science & Technology, Ministry of Education, College of Textiles, Donghua University, Shanghai 201620, PR China

ARTICLE INFO

Article history:
Received 10 September 2016
Revised 13 October 2016
Accepted 15 October 2016
Available online 18 October 2016

Keywords:
Polymer matrix composite
Failure behavior
Damage mechanics
Prepreg

ABSTRACT

Two types of unidirectional carbon fiber reinforced plastic were fabricated using identical carbon fibers but different matrix systems. Thermoplastic polyamide 6 and thermosetting epoxy were used as matrices. A large number of on-axis tensile tests of unidirectional carbon fiber reinforced polyamide 6 (CF/PA6) and the unidirectional carbon fiber reinforced epoxy (CF/Epoxy) laminates were performed. Mechanical properties and failure behaviors are discussed based on fiber distribution, impregnation conditions and interfacial shear strength. Tensile strengths were predicted by means of a modified global load sharing model and compared with experimental results. Step-by-step tensile tests revealed the fracture process of 0-degree unidirectional CF/PA6 laminates.

1. Introduction

Carbon fiber reinforced plastics (CFRPs) have been used in an extensive range of engineering applications because of their outstanding mechanical properties, which enable lightweight and extended service-life structures [1–5]. Metallic materials have gradually been replaced by CFRP [6–9]. It is well known that the mechanical properties of a CFRP are affected by various factors such as the properties of the fiber and matrix, the fiber volume fraction, fiber distribution, impregnation of the matrix, and compatibility between the fiber and the resin (interface and interphase). Manufacturing processes such as temperature, pressure, and process time also affect the mechanical properties. Therefore, many methods to improve the mechanical properties of CFRPs such as fiber treatment [10–12], post-treatment [7,9], structure optimization [7,9,13–15], and micro- or nano-scale filler doping [16–21] have been investigated. One of the most efficient ways to ameliorate the capability of CFRPs is to choose an appropriate surface treatment to improve interfacial strength between the fibers and the matrix.

During loading of a unidirectional (UD) CFRP, mesoscopic events, such as matrix cracking and fiber breakage, initiate and propagate progressively. Such damage accumulates with increased loading. Fiber breakage and matrix cracking often cause interfacial de-bonding [22]. A firm adhesive interface (ideal impregnation of matrix and strong bonding between fibers and matrix) is necessary for the efficient transfer of stress throughout the interface [23]. Modification of the interface could affect fracture modes of a UD CFRP, resulting in disparate mechanical properties [24–28]. The fracture process of a UD CFRP is not currently well understood because the process is extremely rapid (>500 m/s [29]). Ultimate failure of a UD CFRP always occurs abruptly after initiation of mesoscopic events, without any symptoms or visible signs of damage serving as an alarm.

Analytical modeling of tensile failure of a UD CFRP, followed by fiber fragmentation is well established. A useful baseline is obtained by assuming that stress re-distribution around broken fiber follows global load sharing (GLS) [30,31]. This approach assumes that the load from a broken fiber is shared uniformly and equally to all remaining intact fibers across the cross-section of the break point [30–44]. Curtin [30,31] was the first to develop an analysis of the stress–strain response of a fragmenting bundle,

* Corresponding author.
E-mail addresses: stonemayan0416@gmail.com (Y. Ma), ueda.masahito@nihon-u.ac.jp (M. Ueda), yokozeki@aastr.t.u-tokyo.ac.jp (T. Yokozeki), toshi@maruhati.co.jp (T. Sugahara), amy_yuqiu_yang@dhu.edu.cn (Y. Yang), hhamada@kit.ac.jp (H. Hamada).

http://dx.doi.org/10.1016/j.compstruct.2016.10.037
0263-8223/

based on the Cox's [32] shear lag model, Rosen's [33] chain of bundle concept and the Kelly–Tyson [34] approximation model for inefficient length. Curtin's model was later extended by Neumeister [35,36] to account in an approximate way for the overlap of influence zones adjacent to fiber breaks, and subsequently an exact solution to the fragmentation problem was developed. Further research using the GLS model has mainly focused on investigating mechanical behavior, the influencing factors and mechanisms [37–44].

In the present study, a typical thermoplastic resin, polyamide 6 (PA6) and a thermosetting epoxy resin were used as matrices to fabricate UD carbon fiber reinforced PA6 laminates (CF/PA6) and epoxy laminates (CF/Epoxy) through hot compression molding. Their failure behaviors and mechanical properties were investigated based on the fiber distribution, impregnation conditions and interfacial shear strength (IFSS). The modified GLS model was used to predict tensile strengths, which were then compared with experimental results.

2. Experimental methods

2.1. Materials

2.1.1. Production of unidirectional composites

Two types of UC CFRP were fabricated using one type of carbon fiber and different matrix systems. Two UD prepreg sheets were prepared from carbon fibers (T700SC 12K, Toray, Tokyo, Japan) with PA6 (MXD-PA, Mitsubishi Gas Chemical, Tokyo, Japan), and carbon fibers (T700SC 12K, Toray) with epoxy (MCP939, Maruhachi Corporation, Fukui, Japan). The mechanical properties of the raw materials are shown in Table 1. The thickness of a single ply lamina was about 0.1 mm. CFRP laminates with a thickness of 1 mm were fabricated by laminating 10 plies of prepreg sheets with stacking sequences of $[0]_{10}$ for 0-degree longitudinal tensile tests. Molding conditions were 280 °C for 3.5 min under a compression pressure of 4 kg/cm^2 for CF/PA6 laminates and 130 °C for 50 min under a compression pressure of 25 kg/cm^2 for CF/Epoxy laminates. Similarly, laminates with thickness of 2 mm and stacking sequences of $[0]_{20}$ were prepared for transverse tensile tests. Specimens of both CF/PA6 and CF/Epoxy laminates were cut with a size of $15 \times 250 \times 1$ and $25 \times 15 \times 02$ (Width × Length × Thickness: *mm*) for longitudinal and transverse tensile tests, respectively. Rectangular-shaped aluminum-alloy tabs were bonded on both ends of the specimens using an epoxy adhesive (Araldite™), as shown in Fig. 1.

2.1.2. Sample preparation for microindentation tests

From the UD composites, specimens of about 2 mm × 25 mm were cut out and embedded standing upright in a PMMA tube filled with liquid epoxy resin. In this way, an epoxy resin cylinder, containing a sample of CFRPs at the center with fibers in longitudinal direction, is produced. 2 mm thick plate is cut off in order to get a plane perpendicular to the fiber direction.

After cutting, the previously cut face side of the cylinder is grinded and polished by using SiC abrasive paper with grain size from 400, 600, 800, 1200, 1500–2000 step-by-step, then use the aluminum powder with grain size from 1 mm, 0.1 mm to 0.05 mm progressively. For this procedure, the cylinder is clamped in an adapter holding the cylinder perpendicular to the polishing plane. After finishing the first side, the last step in the sample preparation procedure is to grind and polish the second side of the specimen in a similar manner as describe above, till a slice of composite with a thickness of about 100 μm.

2.2. Experimental procedures

2.2.1. Tensile tests

About 60 pieces of 0-degree specimens and more than 10 pieces of 90-degree specimens were prepared. The tensile tests were carried out on a computer-controlled, screw-driven universal testing machine (55R4206, Instron, Kanagawa, Japan) equipped with a 100-kN load cell at a speed of 1 mm/min on the basis of testing standard ASTM D3039 [45]. The tensile tests were performed at room temperature in a relative humidity (RH)-controlled laboratory (23 ± 0.5 °C, 48 ± 2% RH).

2.2.2. Single-fiber push-out tests

Single-fiber push-out tests were performed using a Berkovich Indenter with pyramid geometry (Nano Indenter G200, Agilent Technologies, Oak Ridge, TN, USA), as shown in Fig. 2. The load was applied at a constant rate of 0.2 μm/s. For single-fiber push-out tests, the specimen is required to be thin, to allow fracture over

Table 1
Mechanical properties of materials.

Material	Manufacturer	Type	*E*(GPa)	σ(MPa)	δ.(%)	ρ.(g·cm^{-3})
CF	Toray	T700SC 12 k	230	4900	2.1	1.8
PA6	Mitsubishi Gas Chemical Company	MXD-PA	2.4	82*/48$	4.0*/136$	1.1
Epoxy	Maruhachi Corp.	MCP1110	3.2	80.6	5.4	1.2

E: Tensile modulus;σ: Tensile strength;δ:.Elongation;ρ: Density.
* Yield point.
$ Break point.

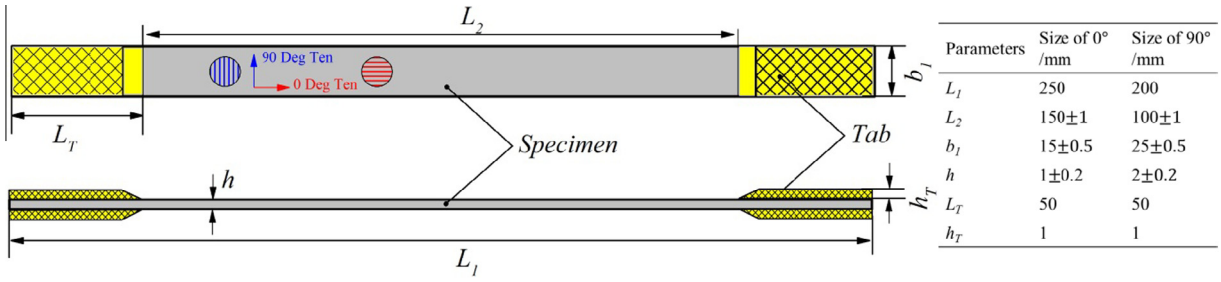

Parameters	Size of 0° /mm	Size of 90° /mm
L_1	250	200
L_2	150±1	100±1
b_1	15±0.5	25±0.5
h	1±0.2	2±0.2
L_T	50	50
h_T	1	1

Fig. 1. Schematic of specimens used for tensile tests, based on the ASTM D3039 standard.

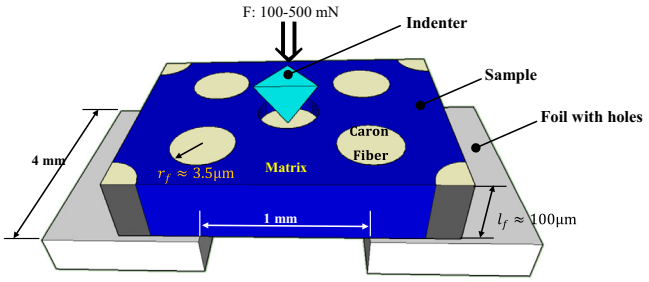

Fig. 2. Illustration of single-fiber push-out tests layout.

the whole interface of the loaded fiber and to push the latter out completely. Prepared thin slice specimens of thickness about 100 μm were placed on an aluminum foil with holes. The specimens were arranged in such a way that a hole was positioned at the position of the loaded fibers, enabling the indenter to push-out the fiber completely into the hole.

The IFSS τ_y is calculated using Eq. (1).

$$\tau_y = \frac{F_{max}}{2\pi r_f l_f} \tag{1}$$

where $F_{\max}$ is the load when interfacial debonding occurs, typically the initial peak load; r_f is the fiber radius (T700S: 3.5 μm); and l_f is the specimen thickness.

2.2.3. Microscope observation

The fiber volume fraction, V_f, was measured on a polished surface of the whole cross-section in a similar way to that described in Ref. [8]. The fiber volume fraction was measured as follows. *(i)* Images taken with an optical microscope (VHX-500F CCD camera, KEYENCE, Osaka, Japan, which has a resolution of 1600 × 1200 pixels) were preprocessed by the aid of *ImageJ* software. *(ii)* Functions in *ImageJ* software "Make Binary" and "Watershed" were used to obtain binary photos, then the function "Noise → Remove outlier" [46] was used to obtain clear boundary carbon fiber images of CF/PA6 and CF/Epoxy laminates. (*iii*) The function "Analyze → Analyze Particles" was used to calculate the area ratio $\left(\frac{\sum^{Fibercrosssection}}{crosssectionofCFRP}\right)$, which is clearly related to the fiber volume fraction because of its UD characteristics. At the same time, the cross-section of specimens was observed to investigate the carbon fiber distribution and crack propagation in CF/PA6 and CF/Epoxy laminates.

2.2.4. Scanning electron microscope observation

All fracture specimens were observed with the optical microscope and then selected samples were coated with an Au-Pd layer and examined in more detail using a scanning electron microscope (SEM, JSM 5200, JEOL, Tokyo, Japan).

3. Modified Global Load Sharing model

The ineffective length δ of a fiber embedded in matrix is defined by Eq. (2) according to the Kelly–Tyson approximation [34].

$$2\delta = \frac{\sigma_f r_f}{\tau_y} \tag{2}$$

where σ_f is the stress in intact fiber. The probability of fiber breakage $P_f(\sigma_f, 2\delta)$ is a function of σ_f and 2δ, and follows a Weibull distribution, as shown in Eq. (3)

$$P_f(\sigma_f, 2\delta) = 1 - exp\left\{-\frac{2\delta}{L_0}\left(\frac{\sigma_f}{\sigma_0}\right)^m\right\} \cong \frac{2\delta}{L_0}\left(\frac{\sigma_f}{\sigma_0}\right)^m \tag{3}$$

where σ_0, m, L_0 are the Weibull scaling parameter, the Weibull modulus and the span length to determine the Weibull parameters, respectively. The analytical derivation of the GLS model is introduced as follows. The matrix axial stress is neglected; namely the composite stress σ_L can be derived as V_f times the fiber sustained stress. The fiber sustained stress can be divided into two components for intact and broken fibers. Thus, the average fiber stress is defined as the sum of stress in the intact fiber times the probability of non-fractured fibers and the recovery stress in the broken fiber times the probability of failure, as indicated in Eq. (4):

$$\begin{aligned}\sigma_L &= V_f\left[\sigma_f\{1 - P_f(\sigma_f, 2\delta)\} + \frac{2\tau_y}{r_f}LP_f(\sigma_f, 2\delta)\right] \\ &= \sigma_f V_f\left\{1 - \left(1 - \frac{L}{\delta}\right)P_f(\sigma_f, 2\delta)\right\}\end{aligned} \tag{4}$$

L is a parameter governing the stress recovery rate in broken fibers. According to the Kelly–Tyson approximation [34], the stress recovers linearly from the breakage point. Curtin [30,31] hypothesized that the average distance from the fiber breakage is half of δ, as described in Eq. (5).

$$\mathrm{L} \cong \frac{\delta}{2} \tag{5}$$

Taketa [47] improved this hypothesis by taking into account the possible positions of the fiber fracture in the range of 2δ. L in Eq. (5) could then be modified as

$$\mathrm{L} \cong \frac{7\delta}{12} \tag{6}$$

Combining Eqs. (2), (4) and (6), the constitutive expression for composite strength can be predicted, as shown in Eq. (7) [47]

$$\sigma_L = \sigma_f V_f\left(1 - \frac{5}{12}\left(\frac{\sigma_f}{\sigma_1}\right)^{m+1}\right) \tag{7}$$

where

$$\sigma_1 = \left(\frac{\sigma_0^m L_0 \tau_y}{r_f}\right)^{\frac{1}{m+1}} \tag{8}$$

$$\sigma_f = \sigma_1\left(\frac{12}{5m+10}\right)^{\frac{1}{m+1}} \tag{9}$$

Then, maximizing with respect to the strain yields, the ultimate tensile strength is

$$\sigma_L^* = V_f\sigma_1\left(\frac{12}{5m+10}\right)^{\frac{1}{m+1}}\left(\frac{m+1}{m+2}\right) \tag{10}$$

To construct a stress–strain curve, the linear relationship between fiber stress and composite strain shown in Eq. (11) can be substituted into above equations, where E_f is the fiber modulus.

$$\sigma_f = E_f\varepsilon_f \tag{11}$$

4. Results and discussion

4.1. Fiber distribution

The cross-section of 0-degree CF/PA6 and CF/Epoxy laminates are shown in Fig. 3(a) and (a') and in Fig. 3(b) and (b'), respectively. CF/Epoxy laminates exhibited a more uniform fiber distribution than CF/PA6 laminates. CF/PA6 laminates exhibited a biased/inhomogeneous fiber distribution; a "bundle"-like fiber agglomeration was observed. Poor fiber impregnation areas internally, with fiber concentrations, were observed in CF/PA6 laminates, as shown in Fig. 3(a'). The difference in fiber distribution between the two

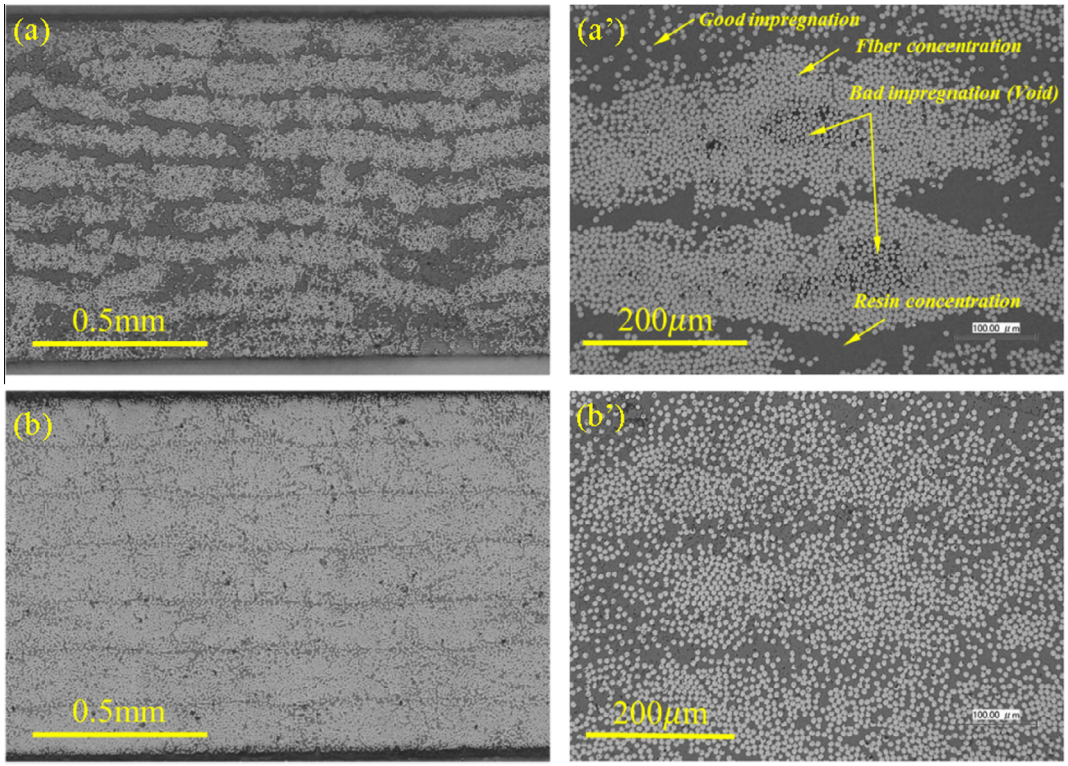

Fig. 3. Cross-section of CF/PA6 laminates at low magnification (a) and high magnification (a') and CF/Epoxy laminates at low magnification (b) and high magnification (b'). Poor impregnation areas and resin concentration areas in CF/PA6 laminates can be observed in (a').

systems (CF/PA6 and CF/Epoxy) is that epoxy wets the fibers at the pre-polymer stage, while the PA6 resin is already polymerized during the fiber impregnation process and its ability to infiltrate the fiber bundles is much lower than that of the unreacted epoxy resin.

4.2. Fiber volume fraction

Because of their UD character, the fiber volume fraction of CF/PA6 and CF/Epoxy laminates were calculated according to the cross-sectional ratio between fibers and laminates, which could be measured by image analysis software (*ImageJ* software) as explained in Section 2.2.3. The results of more than 30 specimens showed the V_f values for CF/PA6 and CF/Epoxy laminates were 42.3% (C.V. ≈8.8%) and 46.5% (C.V. ≈7.7%), respectively.

4.3. Interfacial shear strength

The IFSS was approximated by the average shear strength given by Eq. (1). The IFSS results for CF/PA6 laminates and CF/Epoxy laminates are shown in Fig. 4. For CF/PA6 laminates, two kinds of typical areas including a fiber concentration area (CF/PA6-A: poor impregnation) and a single fiber area (CF/PA6-B: good impregnation) were measured, as shown in Fig. 4(a). The results show that CF/PA6 laminates with good fiber impregnation (IFSS≈18.0 MPa) exhibited higher IFSS than CF/Epoxy laminates (IFSS≈15.0 MPa). However, the CF/PA6 laminates without good fiber impregnation (IFSS≈7.6 MPa) exhibited lower IFSS than CF/Epoxy laminates. The lower IFSS area was dominant and was much larger than the higher IFSS area in the cross-section of CF/PA6. The IFSS results measured by the single-fiber push-out tests using the Berkovich Indenter with a pyramid geometry in the present study exhibited a relatively low IFSS than that measured by other testing methods [47–50]. However, a negative effect of poor impregnation on the IFSS of CF/PA6 laminates could be observed.

4.4. Mechanical properties

4.4.1. Longitudinal loading

Mechanical properties of CF/PA6 and CF/Epoxy laminates are summarized in Table 2. Calculated stress–strain curves of 0-degree laminates from the modified GLS model and typical experimental stress–strain curves (CF/PA6: $V_f \approx 0.431$, CF/Epoxy: $V_f \approx 0.475$) are compared in Fig. 5. The basic parameters including Young's modulus, diameter and gage length, Weibull scale and shape parameters, IFSS and fiber volume fraction used in the present calculation are shown in Table 3.

The relationship between V_f and tensile modulus and the relationship between V_f and tensile strength, together with results from the GLS model are shown in Fig. 6(a) and (b), respectively. V_f and tensile modulus exhibited a linear relationship and fitted the rule-of-mixtures prediction well, as shown in Fig. 6(a). The experimental IFSS and that cited from ref [47] were used to predict the strength by the GLS model. Results indicated that the GLS prediction exhibited a good fit to the strength of CF/PA6 laminates. However, the predicted results for CF/Epoxy laminates showed relatively high tensile strengths compared with experimental results because of the relatively low experimental IFSS. The relationship between modulus and strength by tensile tests, together with results from the GLS model are shown in Fig. 7.

The results shown in Table 2 indicate that there was an appreciable scattering of tensile strength. The statistical distribution of composite strengths is usually described by the Weibull equation [51], with the Weibull distribution given by

$$P_F = 1 - exp\left[-\left(\frac{\sigma_f}{\sigma_0}\right)^{\alpha}\right] \tag{12}$$

where P_F is the cumulative probability of failure of a composite at applied tensile strength σ_f, α is the Weibull modulus (Weibull

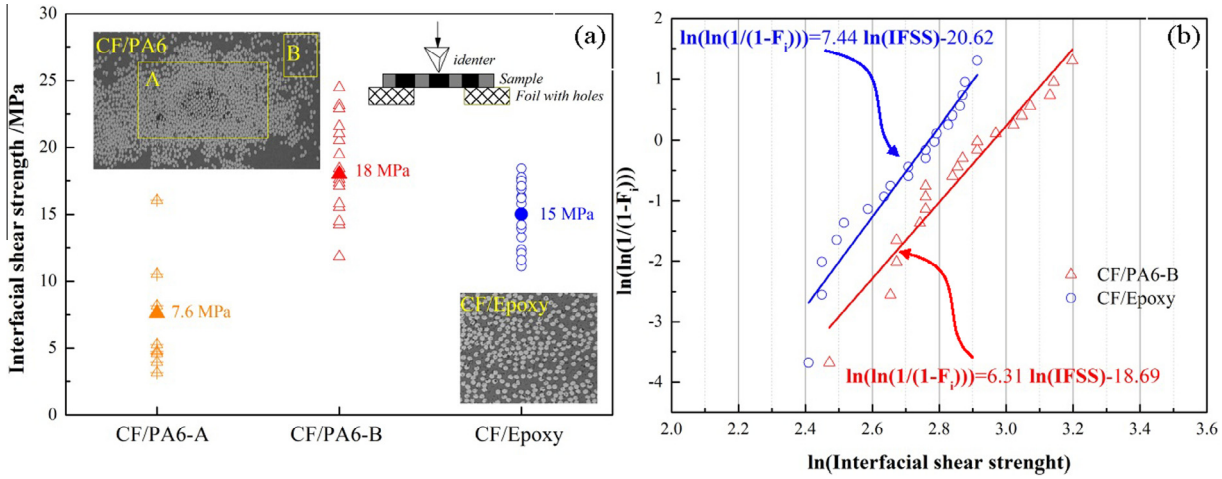

Fig. 4. Interfacial shear strength of CF/PA6 and CF/Epoxy laminates measured by push-out tests (a) and Weibull plots of interfacial shear strength for CF/PA6-B and CF/Epoxy laminates (b).

Table 2
Mechanical properties of unidirectional laminates.

Composites	Alignment	Number	V_f (%)		Tensile modulus (GPa)		Tensile strength (MPa)	
			Mean	C.V. (%)	Mean	C.V.(%)	Mean	C.V. (%)
CF/PA6	0°	59	42.3	8.8	98.2	8.2	1308.9	9.2
CF/Epoxy		67	46.5	7.7	109.1	7.3	1664.0	8.3
CF/PA6	90°	20	–	–	7.4	7.3	33.0	15.7
CF/Epoxy		11	–	–	7.6	6.2	71.8	7.3

C.V.=Coefficient of variation.

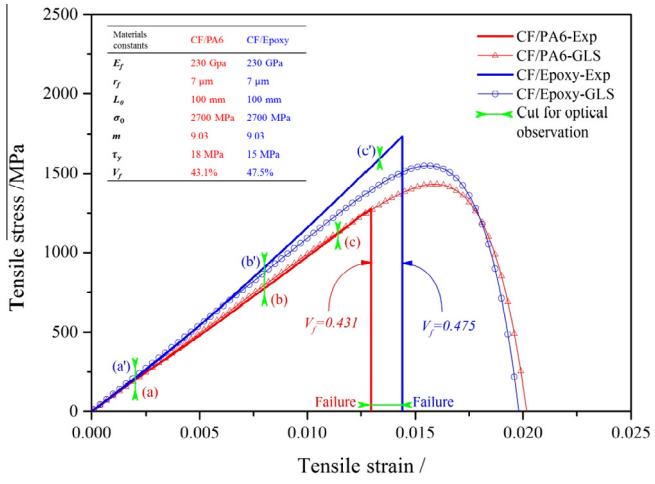

Fig. 5. Typical tensile stress–strain curve comparisons between experiments and predictions from the GLS model.

shape parameter), and σ_0 is a Weibull scale parameter (characteristic stress). Taking the logarithm of both sides of Eq. (12), rearrangement of the two-parameter Weibull statistical distribution expression gives the following:

$$\ln\left[ln(\frac{1}{1-F_i})\right] = \alpha \ln(\sigma_f) - \alpha ln(\sigma_0) \tag{13}$$

Hence the Weibull modulus α can be obtained by linear regression from a Weibull plot of Eq. (13). The probability of failure F_i at the i^{th} ranked specimen from a total of N specimens is obtained from the symmetric rank method as

Table 3
Material constants used in calculations.

Material constants	CF/PA6	CF/Epoxy
Young's modulus of fiber (E_f)	230 GPa[#]	230 GPa[#]
Diameter of fiber (r_f)	7 μm[#]	7 μm[#]
Fiber gage length (L_0)	100 mm[*]	100 mm[*]
Weibull scale factor (σ_0)	2700 MPa[*]	2700 MPa[*]
Weibull shape factor (m)	9.03[*]	9.03[*]
Interfacial shear strength (τ_y)	18 MPa	15 MPa
Fiber volume fraction (V_f)	42.27%	46.50%

[#] From Tory Corp;
[*] Cited from Ref [47].

$$F_i = \frac{i-0.5}{N} \tag{14}$$

where i is rank of the specimen from lowest to highest strength.

The Weibull plots of tensile strength for 0-degree UD CF/PA6 and CF/Epoxy laminates are shown in Fig. 8(a). The Weibull modulus α for 0-degree CF/PA6 and CF/Epoxy laminates were calculated to be 13.3 and 14.9, respectively. The difference in Weibull modulus can be attributed to the distribution of the flaws that exist in the composites. It is well known that many defects are formed in a carbon fiber during precursor manufacturing and various subsequent treatments. The existence of these defects, including fiber misalignment, void and non-impregnation in UD composites results in scattering of the tensile strength. As a result, the Weibull modulus can be regarded as a defect frequency distribution factor [51]. High values of α indicates that there are few defects and they are evenly distributed throughout the material. Low values of α indicates more defects that are less evenly distributed, causing a greater scatter in strength [52].

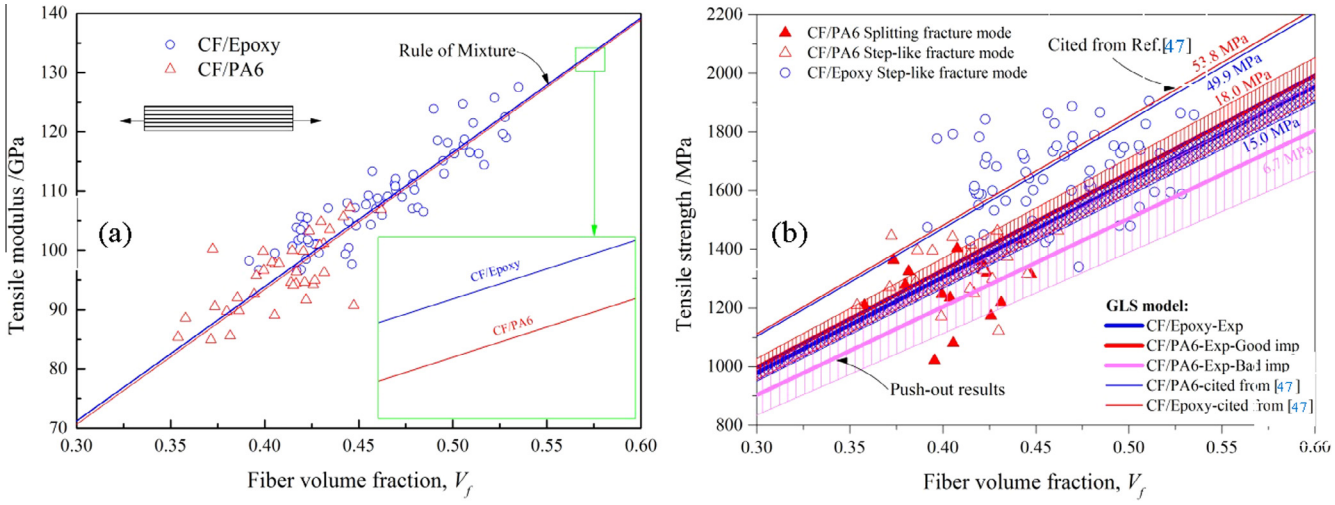

Fig. 6. (a) Relationship between V_f and modulus for both CF/PA6 and CF/Epoxy laminates. The continuous line represents the predicted V_f and modulus relation using the rule-of-mixtures. (b) V_f and tensile strength for both CF/PA6 and CF/Epoxy laminates. The continuous lines represent the predicted V_f and modulus relation using the modified GLS model. The shaded area indicates the scattering of predicted tensile strength using the GLS model, based on the experimental interfacial shear strength results.

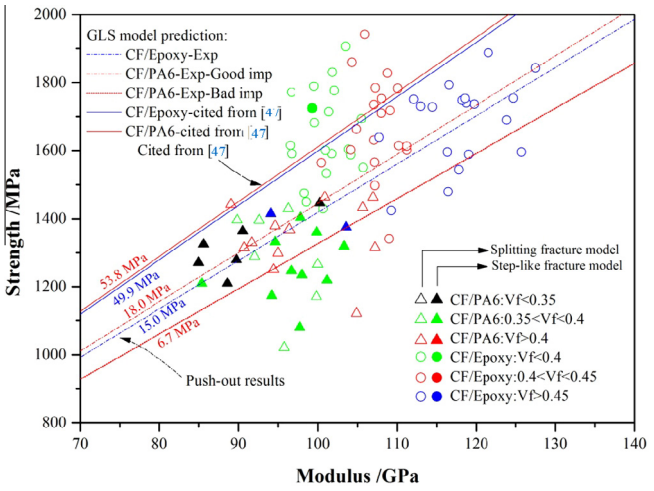

Fig. 7. Relationship between tensile modulus and tensile strength of CF/PA6 and CF/Epoxy laminates with different fiber volume fractions.

4.4.2. Transverse loading

Mechanical properties of 90-degree UD CF/PA6 and CF/Epoxy laminates are shown in Table 2. Results indicate that the transverse tensile strengths of CF/Epoxy laminates were more than double those of CF/PA6 laminates. The Weibull plots of tensile strength for 90-degree UD CF/PA6 and CF/Epoxy laminates are shown in Fig. 8(b). The Weibull modulus α for 90-degree CF/PA6 and CF/Epoxy laminates were 7.5 and 16.0, respectively. According to the IFSS and the transverse strength of UD CF/PA6 and CF/Epoxy laminates, it could be inferred that the poor impregnation of CF/PA6 laminates had negative effects on the mechanical properties and their stabilities.

4.5. Fracture behavior

After tensile tests, two typical fracture modes, including splitting and the step-like mode, of both CF/PA6 and CF/Epoxy laminates were observed, as shown in Fig. 9. Specimens fractured in the step-like mode showed a smoother fracture surface (as shown in Fig. 9(a) and (b)), while specimens fractured in splitting mode

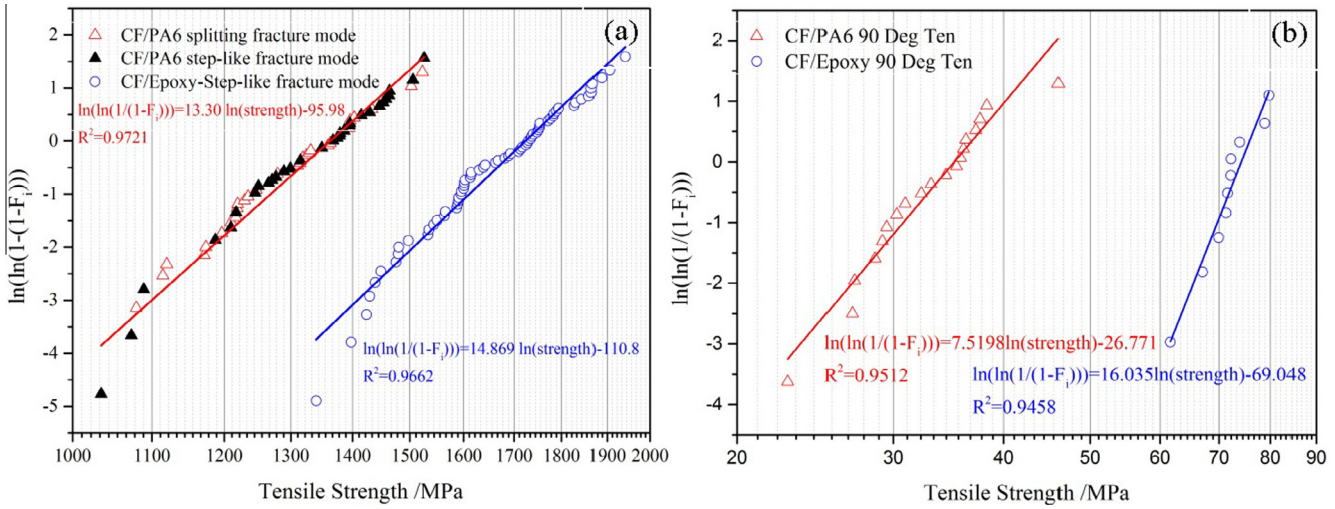

Fig. 8. Weibull plots of tensile strength for 0-degree (a) and 90-degree (b) unidirectional CF/PA6 and CF/Epoxy laminates. Fracture modes, including splitting and step-like fracture modes for 0-degree CF/PA6 and CF/Epoxy laminates after tensile tests are marked in (a).

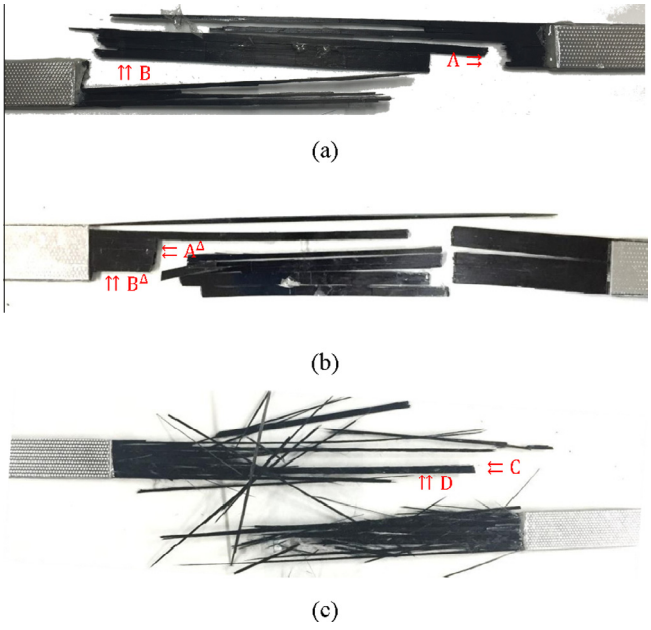

Fig. 9. Two typical fracture modes of CF/PA6 and CF/Epoxy laminates. (a) Step-like fracture mode of CF/PA6 laminates; (b) Step-like fracture mode of CF/Epoxy laminates; (c) Splitting fracture mode of CF/PA6 laminates.

exhibited a broom-like head (as shown in Fig. 9(c)). The main difference was that 0-degree CF/Epoxy laminates all showed the step-like fracture mode after tensile tests, while CF/PA6 laminates exhibited not only step-like fracture modes (≈54.7%) but also the splitting fracture mode (≈45.3%). The fracture behavior distribution of CF/PA6 laminates are shown in Figs. 6(b), 7 and 8(a). There is no evident relationship between the fracture mode and mechanical properties.

4.6. Step-by-step optical observation

To investigate the fracture process in both CF/PA6 and CF/Epoxy laminates, step-by-step tensile tests were carried out. In detail, tensile tests were stopped at strains of 0.2%, 0.8% and 1.2% for CF/PA6 laminates and 0.2%, 0.8% and 1.3% for CF/Epoxy laminates, as shown in Fig. 5. The corresponding polished cross-sections and side-sections of CF/PA6 and CF/Epoxy laminates are shown in Figs. 10 and 11, respectively.

For CF/PA6 laminate, the crack initiated from the fiber concentration areas first (strain≈0.2%), as shown in Fig. 10(a). With an increase in tensile strain (strain ≈ 0.8%), the crack propagated into the fiber concentration areas with little fiber breakage and then along the fiber concentration areas with greater fiber breakage (strain ≈ 1.2%), as shown in Fig. 10(b) and (b') and Fig. 10(c) and (c'), respectively. However, there was no obvious stiffness degradation in the stress–strain relation of CF/PA6 laminates, even though the cracks gradually occurred during the tensile process, as shown in Fig. 5, because of small amount of the damages. In contrast, for CF/Epoxy laminates, there was no obvious crack or fiber breakage up to a tensile strain of 1.3%, as shown in Fig. 11.

The fracture surfaces of CF/PA6 and CF/Epoxy laminates are shown in Fig. 12(a) and (b), respectively. It is clear that more cracks propagated along the fiber concentration areas in CF/PA6 laminates and fractured into small parts. In contrast, most of the cracks in CF/Epoxy laminates propagated along the thickness direction.

Fig. 10 indicates the existence of stress concentration of CF/PA6 laminates. Therefore, modified GLS model may not be adequate in this case, and local load sharing (LLS) model is appropriate alternative. However, the experimental results showed relatively large scatter, which could cause by non-uniform fiber distribution and variation in interfacial strength from place to place. Non-uniform fiber distribution and interfacial strength variation need to be considered to predict scatter in tensile strengths.

4.7. SEM observation

The SEM observation of fracture surfaces along the fiber direction (marked "A⇉" and "⇇A△", as shown in Fig. 9(a) and (b), respectively) of both CF/PA6 and CF/Epoxy laminates in step-like fracture mode are shown in Fig. 13(a) and (b), respectively. It is clear for CF/PA6 laminates that delamination occurred and cracks

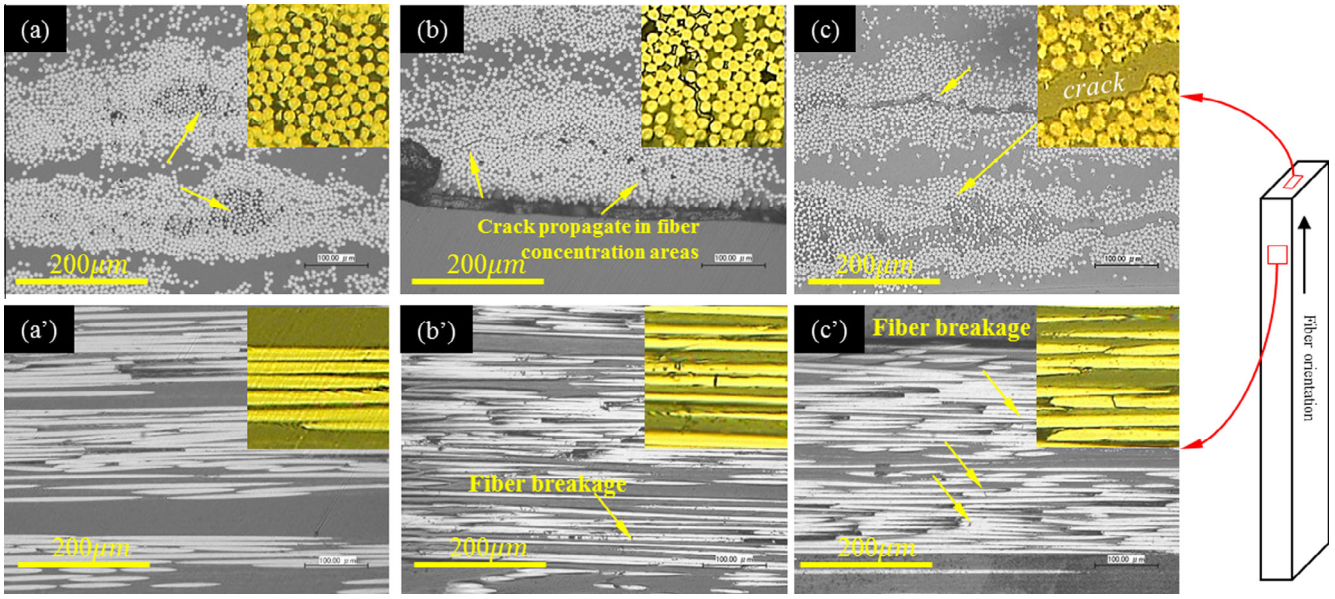

Fig. 10. Crack propagation in CF/PA6 laminates under different axis tensile strain via cross-section and side-section observation. (a) and (a') strain≈0.2%: The first crack initiated from the fiber concentration bundles, in which insufficient bonding existed; (b) and (b') strain≈0.8%: Crack propagated in the concentration areas with little fiber breakage; (c) and (c') strain≈1.2%: Crack propagated along the concentration areas with greater fiber breakage. (a–c) cross-section observation; (a'–c') side-section observation.

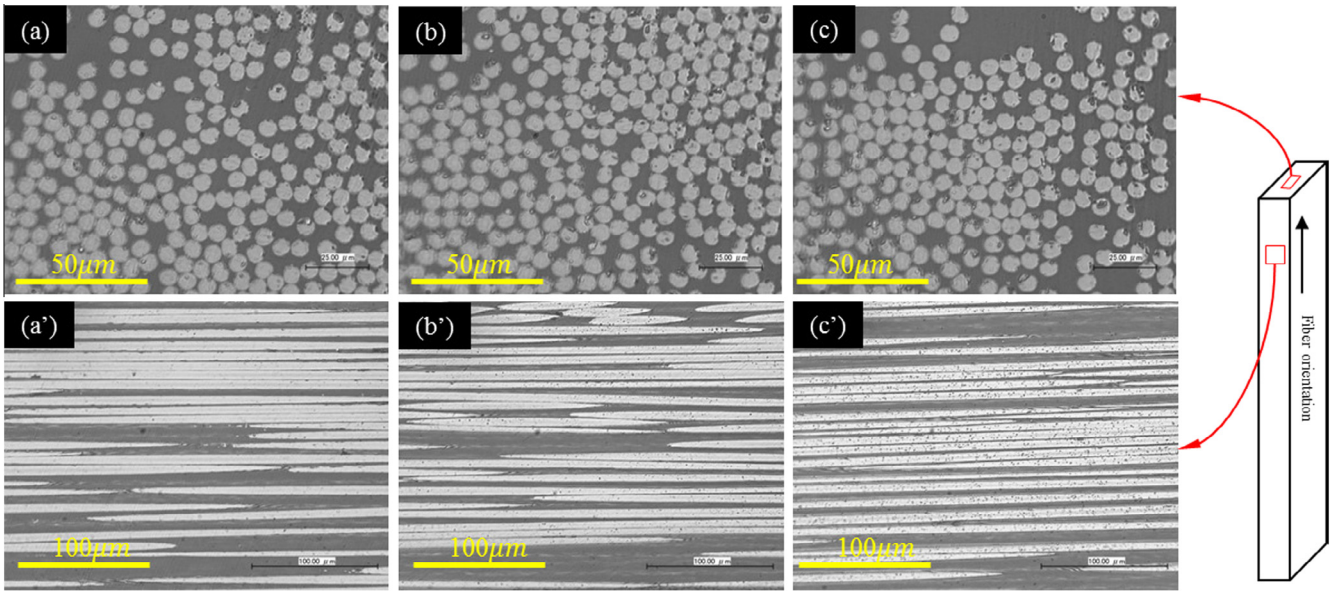

Fig. 11. Cross-sectional observation of CF/Epoxy laminates under different axis tensile strains via cross-section and side-section observation. (a–a') strain ≈ 0.2%, (b–b') strain ≈ 0.8%, (c–c') strain ≈ 1.3%. (a–c) cross-section observation, (a'–c') side-section observation.

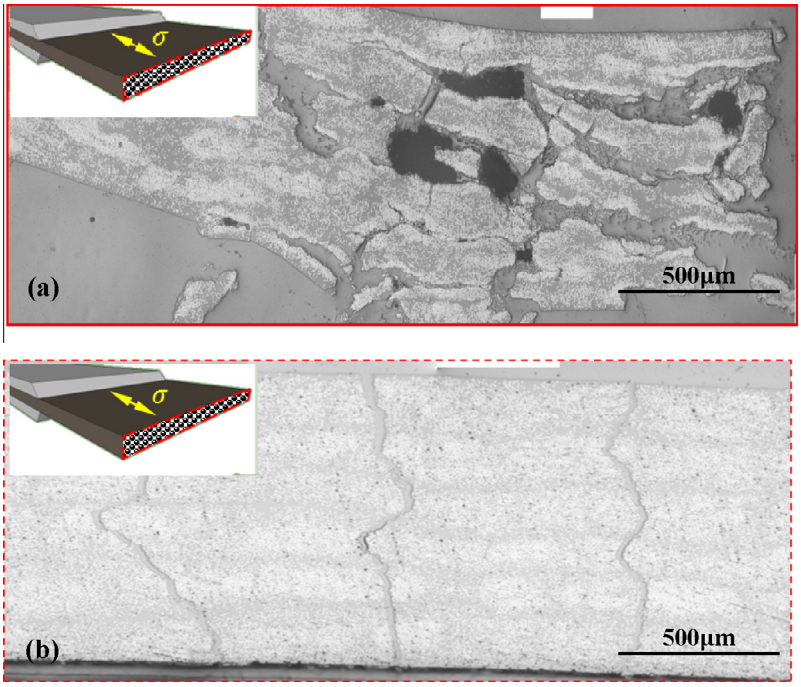

Fig. 12. Cross-section observation of (a) CF/PA laminates and (b) CF/Epoxy laminates after breakage. More cracks propagated along the fiber concentration areas in CF/PA6 laminates and then fractured into small parts. Most of the cracks in CF/Epoxy laminates propagated along the thickness direction.

propagated along the fiber concentration areas, as shown in Fig. 13 (a). However, no delamination occurred and few large-scale cracks and smooth fracture surfaces could be observed in CF/Epoxy laminates, as shown in Fig. 13(b). The SEM observation of the fracture surface vertical to the fiber direction (marked "⇈B" and "⇈B^{Δ}", as shown in Fig. 9(a) and (b), respectively) in both CF/PA6 and CF/Epoxy laminates in step-like fracture mode are shown in Fig. 14 (a) and (b), respectively. It was found that much of the PA6 resin surrounding carbon fibers were torn from fibers, which indicates that cracks propagated mainly in the lower IFSS area. In contrast, for CF/Epoxy laminates, many cracks propagated in the epoxy matrices. These representative characteristics indicate that fracture of CF/PA6 and CF/Epoxy laminates were dominated by interfacial failure and cohesive failure, respectively.

The SEM observation of the fracture surface along (marked "⇇C" as shown in Fig. 9(c)) and vertical to (marked "⇈D" as shown in Fig. 9(c)) the fiber direction of CF/PA6 laminates in splitting fracture mode are shown in Fig. 15(a) and (b), respectively. Similar to the behavior shown in Fig. 13(a), cracks in CF/PA6 laminates propagated along the fiber concentration areas, as shown in Fig. 15(a). Representative interfacial failure (adhesive failure) could be observed in Fig. 15(b).

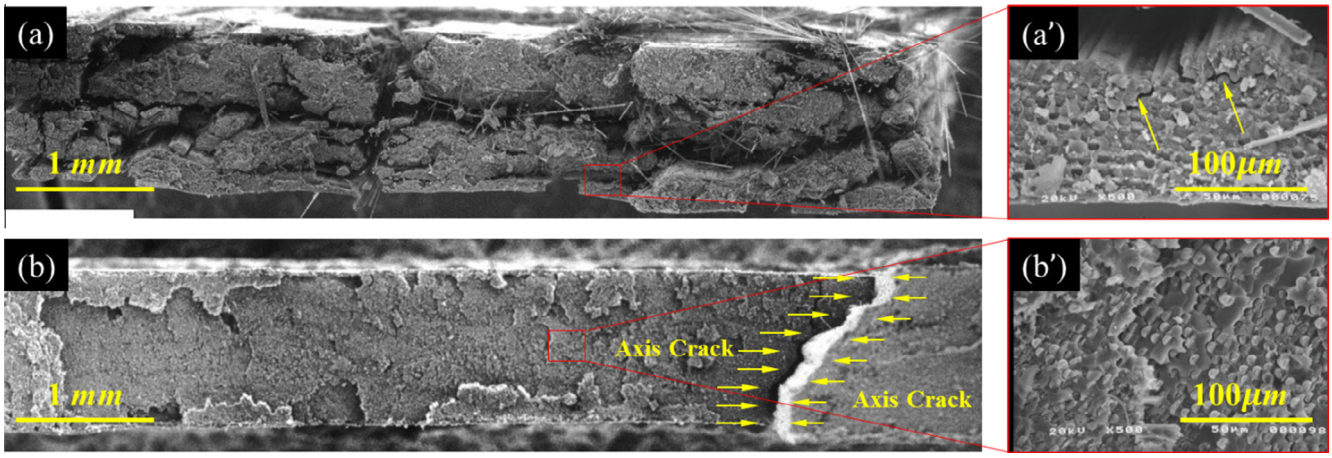

Fig. 13. SEM observation of the fracture surface of (a) CF/PA6 laminates and (b) CF/Epoxy laminates along the fiber direction. Cracks propagated along the fiber concentration areas and delamination occurred in CF/PA6 laminates. No delamination, but axial cracks, occurred in CF/Epoxy laminates.

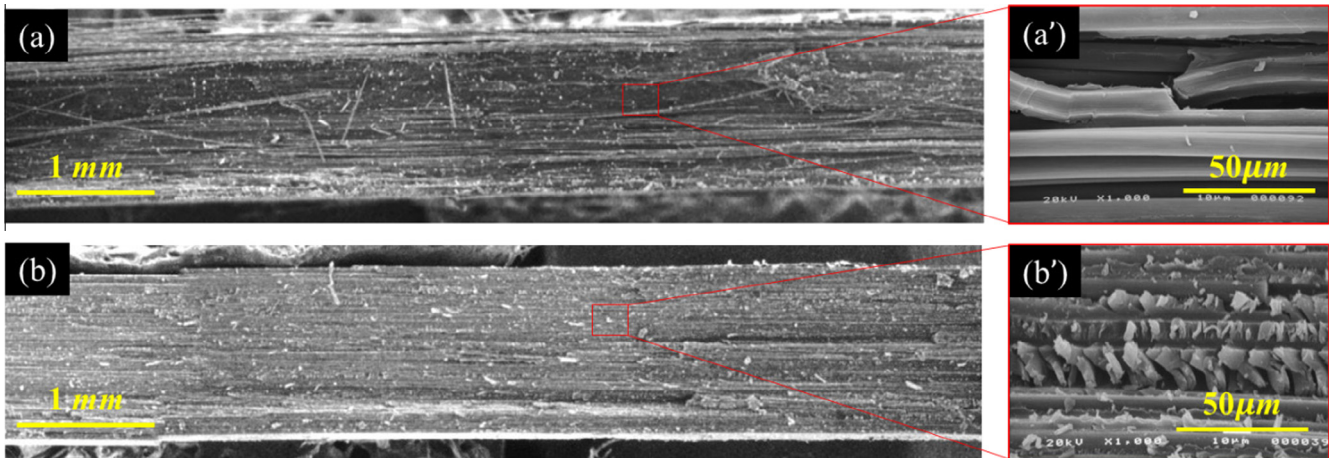

Fig. 14. SEM observation of the fracture surface of (a) CF/PA6 laminates and (b) CF/Epoxy laminates vertical to the fiber direction. (a') Large amounts of PA6 resins surrounding the carbon fibers were torn from the fibers, which could be directly observed in CF/PA6 laminates. In contrast, for CF/Epoxy laminates (b'), many cracks propagated within the epoxy matrices.

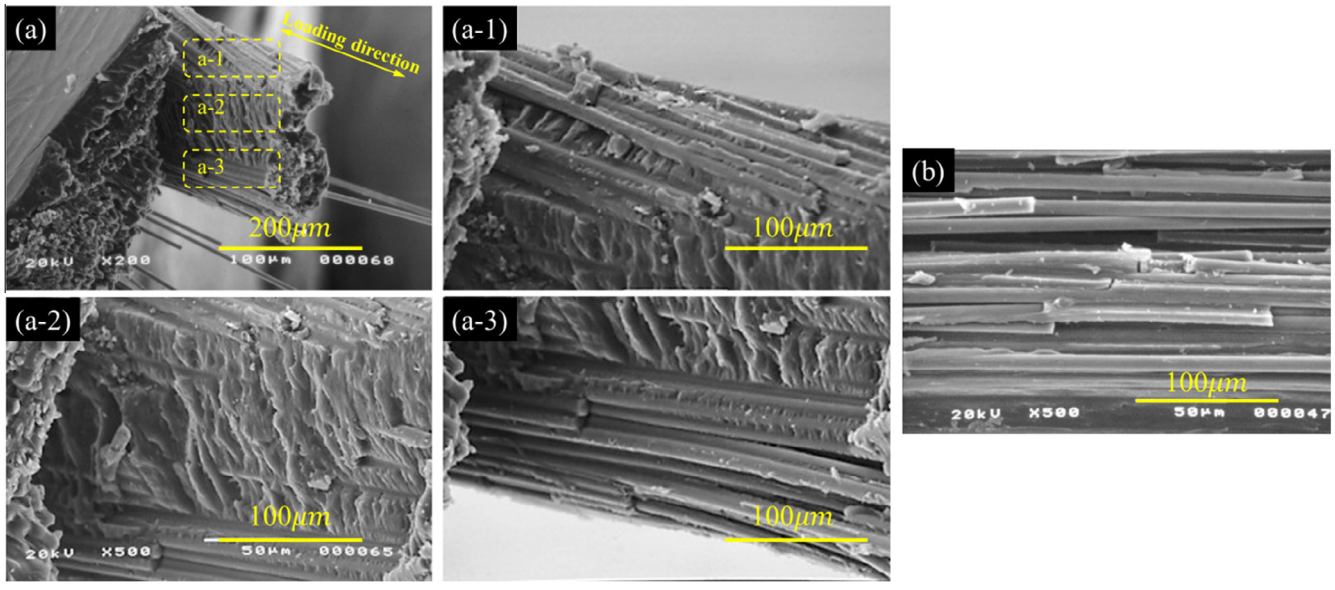

Fig. 15. SEM observation of the fracture surface along and vertical to the fiber direction of CF/PA6 in splitting fracture mode.

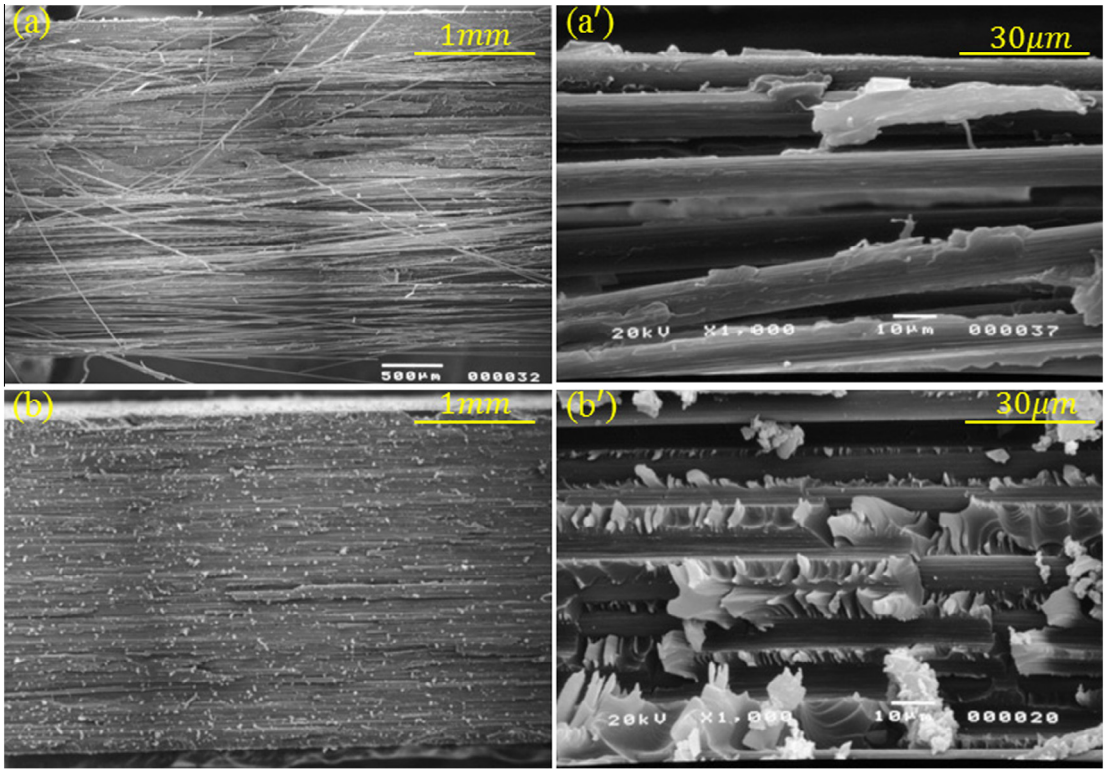

Fig. 16. SEM observation of the fracture surface of 90-degree CF/PA6 (a and a') and CF/Epoxy laminates (b and b') after transverse tensile tests.

The SEM observation of the fracture surface of 90-degree UD CF/PA6 and CF/Epoxy laminates are shown in Fig. 16(a) and (a') and Fig. 16(b) and (b'), respectively. In CF/PA6 laminates, the clean carbon fiber surfaces indicate extensive interfacial failure. Cracks initiated and propagated in the lower IFSS area. In contrast, the carbon fibers in CF/Epoxy laminates are held together by the epoxy matrix. Similar to the shearing fracture mode of 0-degree UD laminates shown in Fig. 14 (observed from the side of "$\uparrow\uparrow B$ and "$\uparrow\uparrow B^{\Delta}$" in Fig. 9(a) and Fig. 9(b), respectively), fracture modes of 90-degree CF/PA6 and CF/Epoxy laminates were dominated by interfacial (adhesive failure) and matrix damage (cohesive failure), respectively.

It is worth emphasizing that although the IFSS of CF/PA6 laminates in some restricted areas were higher than those in CF/Epoxy laminates, cracks initiated and propagated in the ubiquitous lower IFSS area, which resulted in the above extensive interfacial failure in both 0-degree and 90-degree CF/PA6 laminates under tensile tests.

5. Conclusions

Mechanical properties and failure behaviors of a UD carbon fiber reinforced PA6 and epoxy laminates were investigated, based on fiber distribution, impregnation conditions and IFSS. The results obtained can be summarized as follows:

a) Fibers in CF/Epoxy laminates exhibited more uniform distribution than the fibers in CF/PA6 laminates. Epoxy resin wets the fibers at the pre-polymer stage, while the PA6 resin is already polymerized during the fiber impregnation process, and its ability to infiltrate the fiber bundles is much lower than that of the unreacted epoxy resin.
b) CF/PA6 laminates with good fiber impregnation exhibited a higher IFSS than CF/Epoxy laminates. However, CF/PA6 laminates without good fiber impregnation exhibited lower IFSS than CF/Epoxy laminates. The fracture surfaces of 90-degree UD CF/PA6 laminates indicate that cracks propagated mainly in the lower IFSS area, showing interfacial failure. In contrast, the fracture surfaces of 90-degree UD CF/Epoxy showed cohesive failure.
c) The tensile strength of both CF/PA6 and CF/Epoxy laminates follow the Weibull distribution. CF/Epoxy laminates exhibited higher Weibull moduli than CF/PA6 laminates. The modified GLS model prediction exhibited a relatively good fit to the strength of CF/PA6 laminates, while the predictions for CF/Epoxy laminates showed a relative high tensile strength compared with experimental results.
d) Zero-degree UD CF/Epoxy laminates all showed the step-like fracture mode after tensile tests, while CF/PA6 laminates exhibited both step-like and splitting fracture modes.
e) For CF/PA6 laminates with a non-uniform fiber distribution, matrix cracking and fiber breakage were observed before ultimate failure. In contrast, for CF/Epoxy laminates with a uniform fiber distribution, there was no obvious crack or fiber breakage until the tensile strain at ultimate failure.

References

[1] Azeez AA, Rhee KY, Park SJ, Hui D. Epoxy clay nanocomposites–processing, properties and applications: a review. Composites Part B 2013;45(1):308–20.
[2] Dhand V, Mittal G, Rhee KY, Park S-J, Hui D. A short review on basalt fiber reinforced polymer composites. Composites Part B 2015;73:166–80.
[3] Koronis G, Silva A, Fontul M. Green composites: a review of adequate materials for automotive applications. Composites Part B 2013;44(1):120–7.
[4] Ku H, Wang H, Pattarachaiyakoop N, Trada M. A review on the tensile properties of natural fiber reinforced polymer composites. Composites Part B 2011;42(4):856–73.
[5] Ma Y, Zhang Y, Sugahara T, Jin S, Yang Y, Hamada H. Off-axis tensile fatigue assessment based on residual strength for the unidirectional 45° carbon fiber-reinforced composite at room temperature. Composites Part A 2016.
[6] Ma H, Jia Z, Lau K-t, Leng J, Hui D. Impact properties of glass fiber/epoxy composites at cryogenic environment. Composites Part B 2016;92:210–7.

[7] Ma Y, Sugahara T, Yang Y, Hamada H. A study on the energy absorption properties of carbon/aramid fiber filament winding composite tube. Compos. Struct. 2015;123:301–11.
[8] Ma Y, Yang Y, Sugahara T, Hamada H. A study on the failure behavior and mechanical properties of unidirectional fiber reinforced thermosetting and thermoplastic composites. Composites Part B 2016;99:162–72.
[9] Xu J, Ma Y, Zhang Q, Sugahara T, Yang Y, Hamada H. Crashworthiness of carbon fiber hybrid composite tubes molded by filament winding. Compos. Struct. 2016;139:130–40.
[10] Gassan J, Bledzki AK. The influence of fiber-surface treatment on the mechanical properties of jute-polypropylene composites. Composites Part A 1997;28(12):1001–5.
[11] Liu W, Mohanty AK, Askeland P, Drzal LT, Misra M. Influence of fiber surface treatment on properties of Indian grass fiber reinforced soy protein based biocomposites. Polymer 2004;45(22):7589–96.
[12] Rong MZ, Zhang MQ, Liu Y, Yang GC, Zeng HM. The effect of fiber treatment on the mechanical properties of unidirectional sisal-reinforced epoxy composites. Compos. Sci. Technol. 2001;61(10):1437–47.
[13] Awad ZK, Aravinthan T, Zhuge Y, Gonzalez F. A review of optimization techniques used in the design of fibre composite structures for civil engineering applications. Mater. Des. 2012;33:534–44.
[14] Jiang T, Kuila T, Kim NH, Ku B-C, Lee JH. Enhanced mechanical properties of silanized silica nanoparticle attached graphene oxide/epoxy composites. Compos. Sci. Technol. 2013;79:115–25.
[15] Marín L, Trias D, Badalló P, Rus G, Mayugo J. Optimization of composite stiffened panels under mechanical and hygrothermal loads using neural networks and genetic algorithms. Compos. Struct. 2012;94(11):3321–6.
[16] Wetzel B, Haupert F, Zhang MQ. Epoxy nanocomposites with high mechanical and tribological performance. Compos. Sci. Technol. 2003;63(14):2055–67.
[17] Kelnar I, Kotek J, Kaprálková L, Munteanu B. Polyamide nanocomposites with improved toughness. J. Appl. Polym. Sci. 2005;96(2):288–93.
[18] Subramaniyan AK, Sun C. Toughening polymeric composites using nanoclay: crack tip scale effects on fracture toughness. Composites Part A 2007;38(1):34–43.
[19] Xu Y, Van Hoa S. Mechanical properties of carbon fiber reinforced epoxy/clay nanocomposites. Compos. Sci. Technol. 2008;68(3):854–61.
[20] Wei T, Fan Z, Luo G, Wei F. A new structure for multi-walled carbon nanotubes reinforced alumina nanocomposite with high strength and toughness. Mater. Lett. 2008;62(4):641–4.
[21] Lau K-T, Chipara M, Ling H-Y, Hui D. On the effective elastic moduli of carbon nanotubes for nanocomposite structures. Composites Part B 2004;35(2):95–101.
[22] Tanaka M, Hojo M, Hobbiebrunken T, Ochiai S, Hirosawa Y, Fujita K, et al. Influence of non-uniform fiber arrangement on tensile fracture behavior of unidirectional fiber/epoxy model composites. Compos. Interfaces 2005;12(3–4):365–78.
[23] Chamis C. Mechanics of load transfer at the interface. In: Plueddemann EP, editor. Interfaces in Polymer Composites. San Diego: Academic Press; 1974. p. 33–77.
[24] Keusch S, Queck H, Gliesche K. Influence of glass fibre/epoxy resin interface on static mechanical properties of unidirectional composites and on fatigue performance of cross ply composites. Composites Part A 1998;29(5):701–5.
[25] Selzer R, Friedrich K. Mechanical properties and failure behaviour of carbon fibre-reinforced polymer composites under the influence of moisture. Composites Part A 1997;28(6):595–604.
[26] Boccardi S, Meola C, Carlomagno G, Sorrentino L, Simeoli G, Russo P. Effects of interface strength gradation on impact damage mechanisms in polypropylene/woven glass fabric composites. Composites Part B 2016;90:179–87.
[27] Lu T, Liu S, Jiang M, Xu X, Wang Y, Wang Z, et al. Effects of modifications of bamboo cellulose fibers on the improved mechanical properties of cellulose reinforced poly (lactic acid) composites. Composites Part B 2014;62:191–7.
[28] Lu T, Jiang M, Jiang Z, Hui D, Wang Z, Zhou Z. Effect of surface modification of bamboo cellulose fibers on mechanical properties of cellulose/epoxy composites. Composites Part B 2013;51:28–34.
[29] H. Kusano, Y. Aoki, Y. Hirano, T. Hasegawa, Y. Nagao, Visualization on static tensile test for unidirectional CFRP, in: ICCM-17, Edinburgh.
[30] Curtin W. Exact theory of fibre fragmentation in a single-filament composite. J. Mater. Sci. 1991;26(19):5239–53.
[31] Curtin WA. Theory of mechanical properties of ceramic-matrix composites. J. Am. Ceram. Soc. 1991;74(11):2837–45.
[32] Cox H. The elasticity and strength of paper and other fibrous materials. Brit. J. Appl. Phys. 1952;3(3):72.
[33] Rosen BW. Tensile failure of fibrous composites. AIAA J. 1964;2(11):1985–91.
[34] Kelly A, Tyson WR. Tensile properties of fibre-reinforced metals: copper/tungsten and copper/molybdenum. J. Mech. Phys. Solids 1965;13(6).329in1339-338in2-350.
[35] Neumeister JM. Bundle pullout—a failure mechanism limiting the tensile strength of continuous fiber reinforced brittle matrix composites—and its implications for strength dependence on volume and type of loading. J. Mech. Phys. Solids 1993;41(8):1405–24.
[36] Neumeister JM. A constitutive law for continuous fiber reinforced brittle matrix composites with fiber fragmentation and stress recovery. J. Mech. Phys. Solids 1993;41(8):1383–404.
[37] Beyerlein IJ, Phoenix SL, Sastry AM. Comparison of shear-lag theory and continuum fracture mechanics for modeling fiber and matrix stresses in an elastic cracked composite lamina. Int. J. Solids Struct. 1996;33(18):2543–74.
[38] Landis C, McGlockton M, McMeeking R. An improved shear lag model for broken fibers in composite materials. J. Compos. Mater. 1999;33(7):667–80.
[39] Xia Z, Curtin W. Multiscale modeling of damage and failure in aluminum-matrix composites. Compos. Sci. Technol. 2001;61(15):2247–57.
[40] Xia Z, Curtin W, Okabe T. Green's function vs. shear-lag models of damage and failure in fiber composites. Compos. Sci. Technol. 2002;62(10):1279–88.
[41] Okabe T, Ishii K, Nishikawa M, Takeda N. Prediction of tensile strength of unidirectional CFRP composites. Adv. Compos. Mater. 2010;19(3):229–41.
[42] Okabe T, Nishikawa M, Takeda N, Sekine H. Effect of matrix hardening on the tensile strength of alumina fiber-reinforced aluminum matrix composites. Acta Mater. 2006;54(9):2557–66.
[43] Okabe T, Sekine H, Ishii K, Nishikawa M, Takeda N. Numerical method for failure simulation of unidirectional fiber-reinforced composites with spring element model. Compos. Sci. Technol. 2005;65(6):921–33.
[44] Beyerlein IJ, Phoenix SL. Statistics of fracture for an elastic notched composite lamina containing Weibull fibers—Part I. Features from Monte-Carlo simulation. Eng. Fract. Mech. 1997;57(2):241–65.
[45] Materials ASoT. Standard Test Method for Tensile Properties of Polymer Matrix Composite Materials. ASTM D3039/D3039M-14. West Conshohocken: American Society of Testing Materials; 2014.
[46] Rossoll A, Moser B, Mortensen A. Tensile strength of axially loaded unidirectional Nextel 610™ reinforced aluminium: a case study in local load sharing between randomly distributed fibres. Composites Part A 2012;43(1):129–37.
[47] Taketa I. Analysis of failure mechanisms and hybrid effects in carbon fibre reinforced thermoplastic composites (Ph.D. thesis), 2011.
[48] Liu W, Zhang S, Li B, Yang F, Jiao W, Hao L, et al. Improvement in interfacial shear strength and fracture toughness for carbon fiber reinforced epoxy composite by fiber sizing. Polym. Compos. 2014;35(3):482–8.
[49] Zhu M, Li M, Wu Q, Gu Y, Li Y, Zhang Z. Effect of processing temperature on the micro-and macro-interfacial properties of carbon fiber/epoxy composites. Compos. Interfaces 2014;21(5):443–53.
[50] Sharma M, Gao S, Mäder E, Sharma H, Wei LY, Bijwe J. Carbon fiber surfaces and composite interphases. Compos. Sci. Technol. 2014;102:35–50.
[51] Weibull W. A statistical distribution function of wide applicability. J. Appl. Mech. 1951;103:293–7.
[52] Naito K, Tanaka Y, Yang J-M, Kagawa Y. Tensile properties of ultrahigh strength PAN-based, ultrahigh modulus pitch-based and high ductility pitch-based carbon fibers. Carbon 2008;46(2):189–95.